ChemPubSoc
Europe

| Lanthanides

Extending the Row of Lanthanide Tetrafluorides: A Combined Matrix-Isolation and Quantum-Chemical Study

Thomas Vent-Schmidt,[a] Zongtang Fang,[b] Zachary Lee,[b] David Dixon,*[b] and Sebastian Riedel*[c]

Abstract: Only the neutral tetrafluorides of Ce, Pr, and Tb as well as the $[LnF_7]^{3-}$ anions of Dy and Nd, with the metal in the +IV oxidation state, have been previously reported. We report our attempts to extend the row of neutral lanthanide tetrafluorides through the reaction of laser-ablated metal atoms with fluorine and their stabilization and characterization by matrix-isolation IR spectroscopy. In addition to the above three tetrafluorides, we found two new tetrafluorides, $^3NdF_4$ and $^7DyF_4$, both of which are in the +IV oxidation state, which extends this lanthanide oxidation state to two new metals. Our experimental results are supported by quantum-chemical calculations and the role of the lanthanide oxidation state is discussed for both the LnF_4 and $[LnF_4]^-$ species. Most of the LnF_4 species are predicted to be in the +IV oxidation state and all of the $[LnF_4]^-$ anions are predicted to be in the +III oxidation state. The LnF_4 species are predicted to be strong oxidizing agents and the LnF_3 species are predicted to be moderate to strong Lewis acids.

Introduction

The properties of lanthanides and actinides have sparked substantial interest, particularly with regard to understanding the role of valence d and f orbitals in the bonding of ligands to the metal center. Reactions involving lanthanide atoms exhibit trends across the series because of the presence of electrons in the 4f orbitals, even though 4f electrons are usually considered to be inert in terms of the bonding of molecules containing lanthanides. The chemistry of the lanthanides is mostly dominated by compounds in the oxidation state +III owing to the relative inertness of the 4f electrons caused by the contracted radial distribution and the relatively low energy (stabili-

ty) of these orbitals. The lanthanide trifluorides have been the subject of numerous experimental and theoretical investigations owing to their special electronic structure and the question as to whether their structures have C_{3v} or D_{3h} symmetry.[1–12] There is substantial interest in the formation of novel oxidation states of the lanthanides, notably through the work of Evans and co-workers who have found complexes of Ln in the +II formal oxidation state in contrast to the usual +III oxidation state.[13,14,15] The available work on the +II oxidation state has recently been summarized by Meyer;[16] we note that only a few difluorides are known.[2,17] The +IV oxidation state[18] is known for the tetrafluorides of Ce, Pr, and Tb[19,20,21,22] and some oxides[23] and fluorine oxides. In the case of Ln reacting with OF_2, $LnOF_2$ and $LnOF$ were the two products observed in the argon matrix.[24] The $LnOF$ species always have the Ln in the +III oxidation state and the $LnOF_2$ usually have the Ln in the +III oxidation state with the O in the formal −I oxidation state and a spin on the O. Only a +IV oxidation state for Ce and a mixed +III/IV oxidation state for Pr and Tb show deviations from the +III oxidation state. Solids of the formula M_3LnF_7 (Ln = lanthanide; M = alkali metal) where the $[LnF_7]^{3-}$ anion contains a lanthanide in the formal oxidation state +IV are known for neodymium and dysprosium.[25,26] However, the neutral tetrafluorides NdF_4 and DyF_4 are so far unknown. The reaction of laser-ablated lanthanide atoms with fluorine has so far only been reported for the Pr/F_2 system where the stability of a possible praseodymium pentafluoride was discussed.[27] In this study, we continue the investigation of the Ln/F_2 systems to extend the known neutral lanthanide tetrafluorides. This extends matrix-isolation infrared spectroscopic studies of the lanthanides with CH_3F,[12] CH_2F_2,[28] CHF_3,[29] CH_3OH,[30] and OF_2.[24] In most of these cases, the Ln is in the +III oxidation state, which means that there is usually an un-

[a] T. Vent-Schmidt
Albert-Ludwigs-Universität Freiburg
Institut für Anorganische und Analytische Chemie
Albertstrasse 21, 79104 Freiburg (Germany)

[b] Dr. Z. Fang, Z. Lee, Prof. Dr. D. Dixon
Department of Chemistry, The University of Alabama
Tuscaloosa, Alabama 35487-0336 (USA)
E-mail: dadixon@bama.ua.edu

[c] Prof. Dr. S. Riedel
Freie Universität Berlin, Institut für Chemie und Biochemie
Fabeckstrasse 34–36, 14195 Berlin (Germany)
E-mail: sriedel@fu-berlin.de

paired electron on the C or O. We have used a combination of matrix-isolation infrared spectroscopy and computational chemistry to study the LnF$_4$ compounds.

Experimental and Computational Details

Matrix-isolation experiments

Fluorine (99.8%, Solvay) was premixed with neon (99.999%, Air Liquide) or argon (both 99.999%, Sauerstoffwerk Friedrichshafen) in a stainless steel cylinder. The mixing vessel was connected to a self-made matrix chamber by a stainless steel capillary. The reactants were condensed onto a CsI window cooled to 4 K (neon) or 10 K (argon and fluorine) by using a closed-cycle helium cryostat (Sumitomo Heavy Industries, RDK-205D) inside the vacuum chamber. In experiments using neat fluorine, the fluorine cylinder was cooled to 77 K to freeze out common impurities such as CF$_4$, OF$_2$, COF$_2$, and HF. For the laser-ablation experiments, the 1064 nm fundamental of a Nd:YAG laser (Continuum, Minilite II, 10 Hz repetition rate, 35–50 mJ pulse^{-1}) was used, which was focused onto a rotating lanthanide metal target through a hole in the cold window. The metal targets were polished before use to remove the oxide layer and to avoid oxyfluoride contamination. Infrared spectra were recorded on a Bruker Vertex 70 spectrometer purged with dry air at 0.5 cm^{-1} resolution in the region 4000–430 cm^{-1} by using a liquid-nitrogen-cooled mercury cadmium telluride (MCT) detector. The matrix samples were irradiated by a mercury arc street lamp (Osram HQL 250) with the outer globe removed.

Electronic-structure calculations

The electronic-structure calculations were initially performed at the density functional theory (DFT)[31] level with the hybrid B3LYP[32, 33] exchange-correlation functional with the DFT-optimized DZVP2 basis set[34] on F and the small core relativistic effective core potential (ECP) from the Stuttgart group (ECP28MWB) with corresponding segmented basis set (ECP28MWB_SEG) on the lanthanide metals. There are 28 electrons subsumed in the ECP, leaving the 4s, 4p, 4d, 5s, 5p, 6 s, and 4f (and/or 5d) electrons in the valence space for the Ln. The Ln basis set is of the form (14s, 13p, 10d, 8f, 6g/10s, 8p, 5d, 4f, 2g), and we denote this as the Stuttgart basis set.[35, 36] This combination of basis sets and exchange-correlation functional has been found to work well in our analysis of similar reactions with lanthanides.[12, 24, 28, 29, 30] These calculations were performed on each LnF$_4$ and [LnF$_4$]$^-$ complex with different spin states. In many cases, the DFT results were not satisfactory as discussed below so the calculations were redone at the second-order Møller–Plesset (MP2) level[37, 38] with the above basis set for the Ln and the aug-cc-pVDZ basis set[39] on F. The electronic structure was probed by using the NBO6[40, 41, 42, 43, 44] program. The calculations were done with the Gaussian 09 program system.[45]

Results and Discussion

Matrix experiments

The reaction of the laser-ablated lanthanide atoms with fluorine in excess noble gas yielded the lanthanide trifluorides for all metals and the tetrafluorides for Ce, Pr, Nd, Tb, and Dy as well as possibly the difluorides of Pr, Nd, and Sm. The trifluoride of Sm shows only one fundamental, which is indicative of a D_{3h} symmetric structure whereas CeF$_3$, PrF$_3$, NdF$_3$, TbF$_3$, DyF$_3$, and HoF$_3$ show two frequencies, so they have C_{3v} symmetry within the matrix. Figure 1 shows a comparison of spectra obtained for the investigated Ln/F$_2$ systems in argon whereas Figure 2 compares the neon-based spectra.
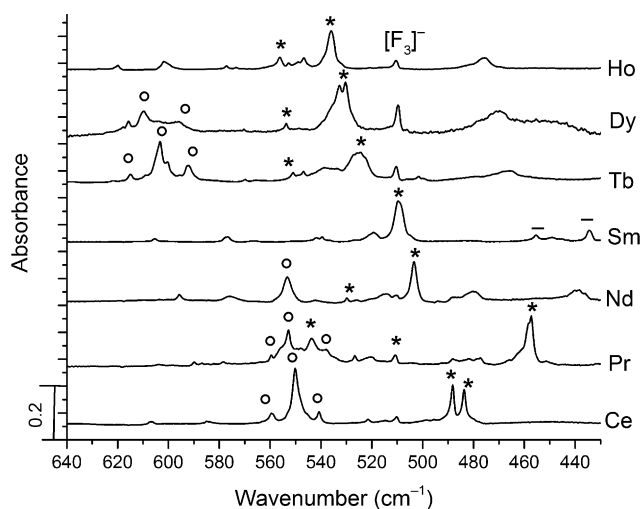
Figure 1. Reaction products of laser-ablated lanthanide atoms with F$_2$ in excess argon. Asterisks mark LnF$_3$ compounds, bars correspond to SmF$_2$, whereas circles mark tetrafluorides. For better comparison, some of the spectra have been scaled.
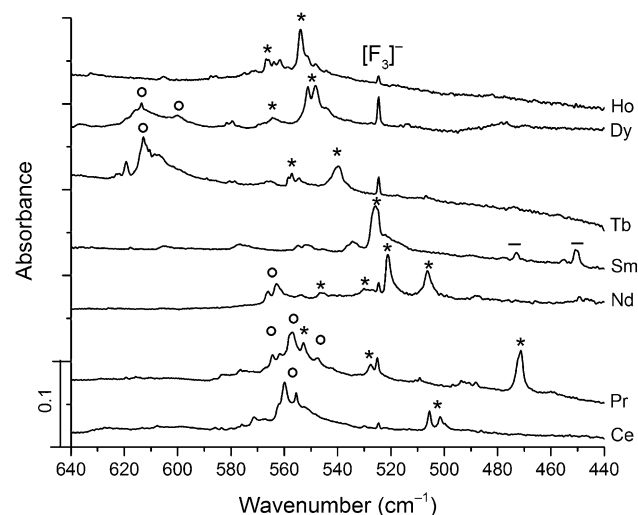
Figure 2. Reaction products of laser-ablated lanthanide atoms with F$_2$ in excess neon. Asterisks mark LnF$_3$ compounds, bars correspond to SmF$_2$, whereas circles mark tetrafluorides. For better comparison, some of the spectra have been scaled.

Table 1. Calculated symmetric (sym) and asymmetric (asym) Ln–F vibrational frequencies (ν, cm^{-1}), and infrared intensities (I, km mol^{-1}, in parentheses) of LnF$_4$ complexes at the B3LYP/Stuttgart/DZVP2 and MP2/Stuttgart/aug-cc-pVDZ levels.

LnF$_4$	Point group	Sym. ν MP2/B3LYP[a]	Asym. ν MP2/B3LYP[a]	Exptl ν[b]
^{2}LaF$_4$	D_{2d}	464.6	554.1 (e) 698.3	
^{1}CeF$_4$	T_d	612.7/586.9 (0)	560.6/556.4 (698)	Ar: 540.7, 550.1, 559.4 Ne: 560.0, 555,6 F$_2$: 542
^{2}PrF$_4$	T_d	619.2/585.3 (0)	574.6/600.5 (377)	Ar: 537.7, 547.6, 552.4 559.1 Ne: 547.0, 556.6, 561.2, 564.0 F$_2$: 550, 534
^{3}NdF$_4$	D_{2d}	625.9/579.8 (0)	576.5/549.8 (179) 586.1 (e)/545.9 (423)	Ar: 542.2, 553.1 Ne: 562.7, 566.0 F$_2$: 545
^{4}PmF$_4$	D_{2d}	632.3/571.2 (27)	588.8 (e)/554.8 (342) 594.5/561.4 (138)	
^{5}SmF$_4$	T_d	638.5	595.2	
^{6}EuF$_4$	D_{2d}	640.2	590.1 (e) 598.1	
^{8}EuF$_4$	C_{2v}	380.3 578.1	546.9 645.7	
^{7}GdF$_4$	C_{2v}	642.2	554.2 593.2 664.9	
^{9}GdF$_4$	D_{2d}	497.0	560.4 (e) 693.6	
^{8}TbF$_4$	T_d	653.3	617.2	Ar: 592.8, 600.1,603.3, 614.5 Ne: 612.9 F$_2$: 586–607
^{7}DyF$_4$	C_{2v}	658.5	616.9 619.8 623.8	Ar: 610.3, 596.8, 602.6, 587.5 Ne: 613.4 F$_2$: 604
^{6}HoF$_4$	D_{2d}	662.8/594.6 (0)	623.1 (e)/590.0 (294) 626.1/583.7 (119)	
^{5}ErF$_4$	C_{2v}	667.7	636.9 637.7 642.3	
^{4}TmF$_4$	T_d	672.6	641.8	
^{3}YbF$_4$	D_{2d}	678.1	648.0 648.8 (e)	
^{2}LuF$_4$	D_{2d}	511.9	628.1 (e) 772.3	

[a] For T_d, the symmetric frequencies are of a$_1$ symmetry and the asymmetric are of t$_2$ symmetry. For D_{2d}, the symmetric stretch is of a$_1$ symmetry and the asymmetric is of e and b$_2$ symmetry. [b] The type of matrix precedes the experimental data.

In all experiments, the previously reported trifluoride anion, [F$_3$]$^-$, could be found at 510.6 in argon and at 524.7 cm^{-1} in neon.[46] In the neon experiments, the recently found [F$_5$]$^-$ anion was also observed at 850.7 cm^{-1}.[47,48] As recently reported by Mikulas et al.,[24] we also checked our spectra for lanthanide oxyfluorides, which might arise from the laser-ablated metal oxides surface with fluorine. However, no bands for the expected LnOF or LnOF$_2$ molecules were found.[24] The following discussion is based on the argon spectra for convenience, although a similar discussion is valid for the neon experiments. All of the values can be found in Table 1.

We first discuss the Ce/F$_2$ system as the Ce can readily attain the +IV oxidation state. Figure 3 shows the reaction products of laser-ablated cerium atoms with fluorine in argon. On sample deposition, a characteristic doublet splitting for the ν_3(E) mode of CeF$_3$ at 488.3 and 483.6 cm^{-1} along with a weaker ν_1(A$_1$) mode at 521.8 cm^{-1} were observed and these agree well with previously reported bands.[11] The strong ν_3(T$_2$) mode of CeF$_4$ is found at 550.1 cm^{-1} with matrix sites at 540.8 and 559.5 cm^{-1} in accordance with prior experimental[49] and computational[50] results. On annealing, the main band at 550.1 cm^{-1} as well as the trifluoride bands decrease and two other bands at 545.4 and 538.4 cm^{-1}, assigned to CeF$_4$ in a different matrix environment (Figure 3 b, c, f, and g), increase. Based on the spectra, it is difficult to determine whether new CeF$_4$ is formed on annealing, which is supported by the decrease of CeF$_3$, or if there is just a matrix reorganization. On irradiation with the full spectrum of a mercury arc, the tetrafluoride is formed at the expense of CeF$_3$ (Figure 3 d and h). On further annealing to 35 K, the matrix begins to evaporate. The formation of CeF$_4$ on photolysis and the decrease of CeF$_3$ during the experiment shows that the tetrafluoride is the most stable fluoride under these conditions.
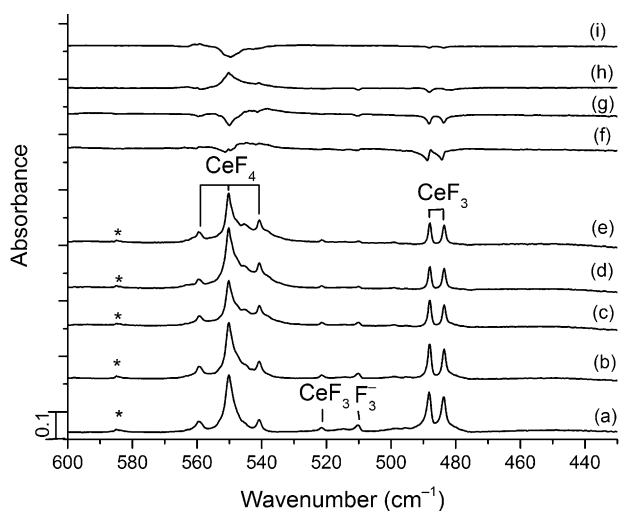
Figure 3. Reaction products of laser-ablated cerium atoms with 2% F_2 in excess argon. (a) Deposition, (b) annealing to 25 K, (c) annealing to 31 K, (d) UV photolysis for 30 min, (e) annealing to 35 K, (f) difference (b)−(a), (g) difference (c)−(b), (h) difference (d)−(c), (i) difference (e)−(d). Asterisks mark unknown metal independent impurities.

The Pr/F_2 system is the subject of a recently published investigation and will not be discussed in detail herein.[27] However, some points are noteworthy for our discussion. The product spectrum of laser-ablated Pr atoms with F_2 shows PrF_4 and PrF_3 as the main products and there is evidence for the low-valent fluorides PrF (Pr^I) and PrF_2 (Pr^{II}). PrF_4 is formed on annealing at the expense of PrF_3 and the tentatively assigned low-valent fluorides. In contrast to CeF_4, praseodymium tetrafluoride decomposes on photolysis and PrF_3 is regenerated.

Figure 4 shows the reaction products of laser-ablated Nd atoms with F_2 in argon. On deposition, known bands for NdF_3 were found at 503.0 and 529.7 cm^{-1}.[11] The new NdF_4 molecule
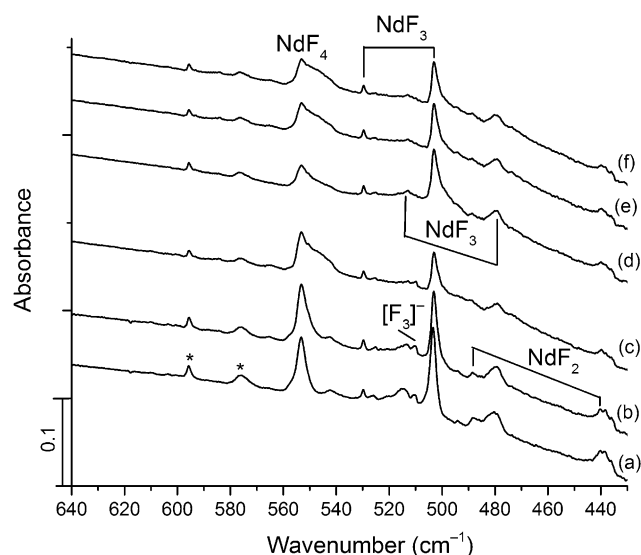
Figure 4. Reaction products of laser-ablated neodymium atoms with 1% F_2 in excess argon. (a) Deposition, (b) annealing to 25 K, (c) annealing to 29 K for 2 min, (d) UV photolysis for 30 min, (e) annealing to 28 K for 2 min, (f) annealing to 35 K. Asterisks mark unknown metal independent impurities.

is found at 553.1 cm^{-1} with a weaker band at 542.2 cm^{-1}. The assignment to the tetrafluoride is made on the basis of three observations. First, on annealing (Figure 4b and c), these bands grow in at the expense of NdF_3, which is characteristic for a higher fluoride. Second, on photolysis (Figure 4d), the compound decomposes and the bands for NdF_3 increase. This behavior is the same as that for PrF_4, but is in contrast to CeF_4, which indicates the lower stability of PrF_4 and NdF_4. Third, the Ln–F stretching frequencies follow the lanthanide contraction. As the Ln–F bonds in the tetrafluorides can be considered as even more ionic than the ones in the trifluorides, the same trend is expected for these compounds. Figures 1 and 2 show that there is a blueshift of 2.3 cm^{-1} from CeF_4 to PrF_4 and of 1.0 cm^{-1} from PrF_4 to NdF_4. These blueshifts are remarkably lower than those observed for the trifluorides.

On annealing, in the Nd/F_2 spectra, a shoulder shifted to lower wavenumbers with respect to the sharp tetrafluoride peak grows in. The band decreases in unison with the band at 533.1 cm^{-1} on photolysis and is reformed after subsequent annealing. We hypothesize that this is not a new compound, but is either a second stable matrix site of NdF_4 or a slightly less stable electronic state, which leads to a small structural change. Additional bands are found at 515.5, 488.3, 479.8, and 439.8 cm^{-1}, of which the 515.5 and the 479.8 cm^{-1} bands track each other. These latter two bands are known from the work of Hauge et al. and can be assigned to another stable matrix site of NdF_3.[10] In neon, two sites are also observed, the $\nu_1(A_1)$ and $\nu_3(E)$ bands are located at 530.1 and 506.7 cm^{-1} as well as at 546.5 and 521.3 cm^{-1} for the second site, which is also in line with the literature.[10] The bands at 488.3 and 439.8 cm^{-1} also seem to track each other and could be tentatively assigned to NdF_2 by comparison with the known bands of SmF_2, which are in the same spectral range and show the same intensity distribution and behavior on annealing and photolysis.

The Sm/F_2 spectrum (Figure 1 and Figure 2) shows no evidence for the formation of a tetrafluoride. The main product band of SmF_3 is observed at 508.7 cm^{-1} and weaker bands for the difluoride are at 455.1 and 434.5 cm^{-1}, both in accordance with literature.[2] SmF_3 is formed on photolysis while the main product band decreases on annealing and weak shoulder bands shifted to lower wavenumbers grow in. These bands, as well as similar bands for the modes observed at 519.3, 539.4, and 541.9 cm^{-1}, were previously found in experiments with Knudsen cell evaporated SmF_3 and can be tentatively assigned to polymer bands.[2]

The chemical behavior on annealing and photolysis of the Tb/F_2 system is the same as for the Ce/F_2 system, which indicates that TbF_4 is the most stable compound in the system under cryogenic conditions. Bands for TbF_3 are found at 523.6 and 550.9 cm^{-1} in accordance with the literature[10] and at 603.3 cm^{-1} for TbF_4, with matrix splittings at 592.8, 596.4, 600.1, and 612.2 cm^{-1}.[22] Additional bands are found at 536.8 and 466.1 cm^{-1}, which could not be assigned. One possibility would be the unknown TbF_2 molecule. However, the bands for this compound are expected to be shifted to lower wavenumbers than TbF_3 and do not match our calculated values. It is

also expect that an unstable difluoride would rapidly vanish on annealing, which is not the case. The chemical behavior also does not fit to a possible charged species. As these bands track with the modes of TbF_3 and as these bands are not observed in neat fluorine experiments, they might belong to the trifluoride dimer or polymers.

The product spectrum of the Dy/F_2 system shows distinctive bands of DyF_3 at 554.0 cm^{-1} ($\nu_1(A_1)$) and a split $\nu_3(E)$ fundamental at 530.6 and 533.0 cm^{-1} (Figure 5).[51,52] Unknown absorptions were found in the region of a possible tetrafluoride at
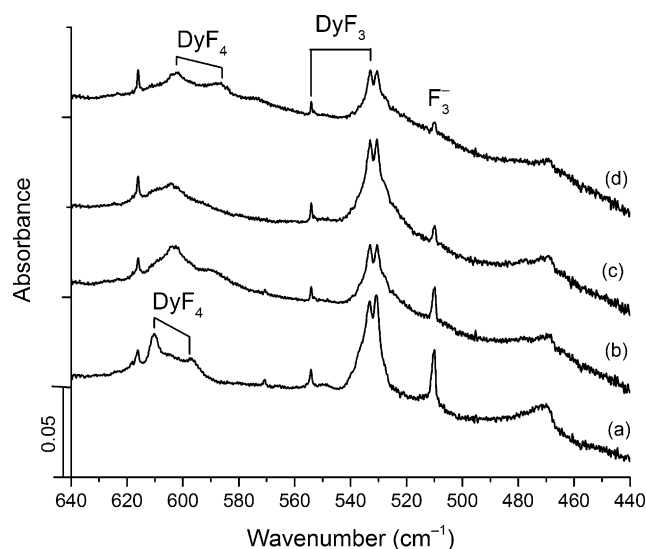
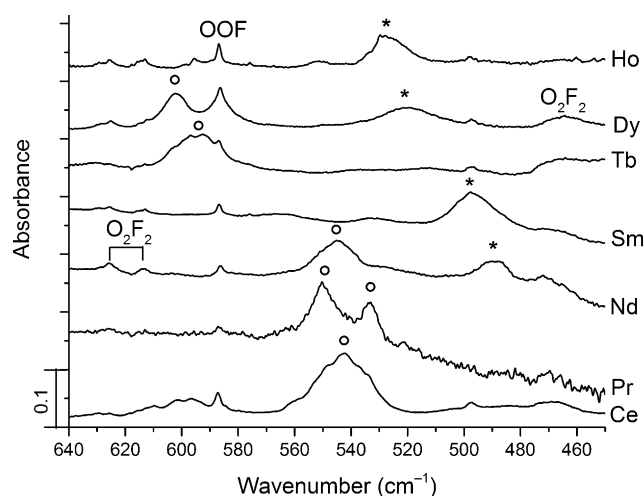**Figure 5.** Reaction products of laser-ablated dysprosium atoms with 2% F_2 in excess argon measured at 0.2 cm^{-1} resolution. (a) Deposition, (b) annealing to 30 K, (c) UV photolysis for 30 min, (d) annealing to 35 K.

610.3 and 596.8 cm^{-1} on deposition. These bands are assigned to the new DyF_4 molecule because they show a reasonable shift compared with TbF_4 as a result of the lanthanide contraction. On annealing, these two bands shift to 602.6 and 587.5 cm^{-1}, which probably can be explained by changes in the electronic structure and a different matrix site, which is supported by the neon experiments in which this shift could not be observed because of the lower annealing temperatures. Owing to this shift, it is difficult to say whether the tetrafluoride bands also increase on annealing, but the decreasing trifluoride bands as well as the second annealing after photolysis (Figure 5 d) give strong evidence for that. On photolysis, the trifluoride bands increase at the expense of the tetrafluoride ones. An additional sharp band is found at 616.0 cm^{-1}, which does not track the tetrafluoride bands and which cannot be assigned to known impurities. As this band is not resolved from the tetrafluoride bands in the neon experiments, the behavior on annealing and photolysis cannot be determined in these experiments and the band has not been assigned. A broad feature is also found at 469 cm^{-1}, which decreases on annealing and might increase slightly on photolysis. On the basis of the calculations described below, this can be assigned to $[DyF_4]^-$. The region would also be characteristic for a difluoride, but there is no evidence for the second mode.

The Ho/F_2 spectrum shows two bands for the trifluoride at 535.8 and 556.6 cm^{-1}, which are also reported in literature.[10] Additional weaker bands are found at 474.7, 532.3, 546.7, 601.6, and 616.7 cm^{-1}, which track the trifluoride fundamentals. Although not assigned, similar bands were also observed in Knudsen cell evaporated HoF_3 spectra and, thus, we assign these bands to polymer species.[10] The behavior on annealing and photolysis of the HoF_3 fundamentals is the same as that for all of the other trifluorides and there is no evidence for a possible tetrafluoride.

Further conformation for the assignment of NdF_4 and DyF_4 comes from experiments using neat fluorine as the matrix material, as shown in Figure 6 and Figure 7. An article describing the properties of a fluorine matrix has recently been published.[47,48] In a neat fluorine matrix, the known tetrafluorides CeF_4, PrF_4, and TbF_4 are the most stable products and the for-

Figure 6. Reaction products of laser-ablated lanthanide atoms with F_2 in neat fluorine. Asterisks mark LnF_3 compounds whereas circles mark tetrafluorides. For better comparison, some of the spectra have been scaled.
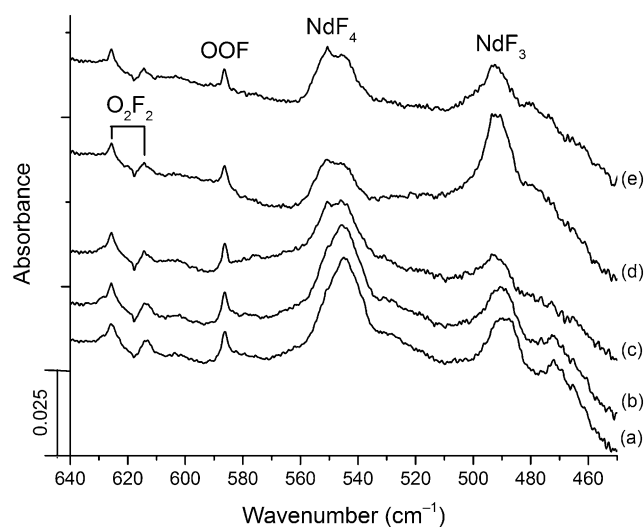
Figure 7. Reaction products of laser-ablated neodymium atoms with F_2 in neat fluorine. (a) Deposition, (b) annealing to 20 K, (c) annealing to 28 K for 2 min, (d) UV photolysis for 30 min, (e) annealing to 30 K.

mation of LnF$_3$ is not observed with these elements. For Ce and Tb, photolysis leads again to the formation of the tetra-fluoride as in the argon and neon experiments. In contrast to the argon and neon experiments where irradiation with the full mercury arc led to decomposition of PrF$_4$ and the formation of PrF$_3$, no significant change in the PrF$_4$ band nor the formation of PrF$_3$ could be observed in the fluorine matrix. On the other hand, in a fluorine matrix, Nd and Dy show significant formation of the trifluoride in addition to the tetrafluoride, indicating the lower stability of NdF$_4$ and DyF$_4$ (Figure 6). Again, there is no evidence for a tetrafluoride of samarium and holmium in our neat fluorine spectra.

Figure 7 shows an exemplary spectrum and the chemical behavior on annealing and photolysis of the products of laser-ablated Nd atoms in a neat fluorine matrix, but the Dy/F$_2$ systems are totally comparable. As expected, the tetrafluoride is formed on annealing as indicated by the decrease of the tri-fluoride in Figure 7b and c, which is clearly supported by the formation of the tetrafluoride on annealing in Figure 7e. On photolysis, the tetrafluoride decomposes to the trifluoride (Figure 7d). The process of destroying the tetrafluoride on photolysis and reforming it on annealing can be cycled several times during the experiment. In these experiments the neat fluorine matrices emerge as a powerful tool to support our assignments made on the basis of the argon and neon spectra.

Computational results

The LnF$_4$/[LnF$_4$]$^-$ sequence can be thought of as adding an F$^{\bullet}$ radical or an F$^-$ to LnF$_3$ and the question then exists as to whether the LnF$_3$ will change its oxidation state on addition of

the F$^{\bullet}$/F$^-$. In addition, the ability to add F$^-$ is a measure of the Lewis acidity of the LnF$_3$.

Geometries

Two additional point groups derived from the ideal T$_d$ point group with at least a C_2 axis and a mirror plane are possible for the LnF$_4$ complexes: C_{2v} and D_{2d} and these are the point groups predicted for distorted molecules. The bond lengths, angles, and symmetries of the LnF$_4$ are given in Figure 8. All of the tetrafluorides are predicted to be minima. The MP2 geometries follow, in most cases, the lanthanide contraction, which suggests that the Ln–F bonds should decrease moving from left to right across the series. The exceptions are the high spin states for EuF$_4$ (octet), GdF$_4$ (nonet), and the final member, LuF$_4$. LaF$_4$ is predicted to have the longest bond length of the LnF$_4$ at 2.141 Å, which is consistent with the fact that it is the earliest lanthanide in the series and also cannot have an oxidation state beyond +III. It is significantly distorted from the T$_d$ geometry to D_{2d} symmetry with bond angles of 90° and 120°. ^{8}EuF$_4$ is slightly more stable than ^{6}EuF$_4$ by 5.3 kcal mol^{-1} and ^{9}GdF$_4$ is more stable than ^{7}GdF$_4$ by 53.0 kcal mol^{-1}. The more stable high-spin ^{8}EuF$_4$ and ^{9}GdF$_4$ have longer bond lengths than do the low-spin ^{6}EuF$_4$ and ^{7}GdF$_4$. The Ln–F bond lengths in the low-spin ^{6}EuF$_4$ and ^{7}GdF$_4$ follow the lanthanide contraction. The reason for the longer bond lengths in the high-spin compounds is that they are in the +III oxidation state as discussed below. The lower spin compounds follow the lanthanide contraction because they are in the +IV oxidation state. The largest angle distortions are for ^{8}EuF$_4$ with bond angles of 110° between the two longer bonds and 137° between the shorter bonds. The remaining molecules show smaller angular
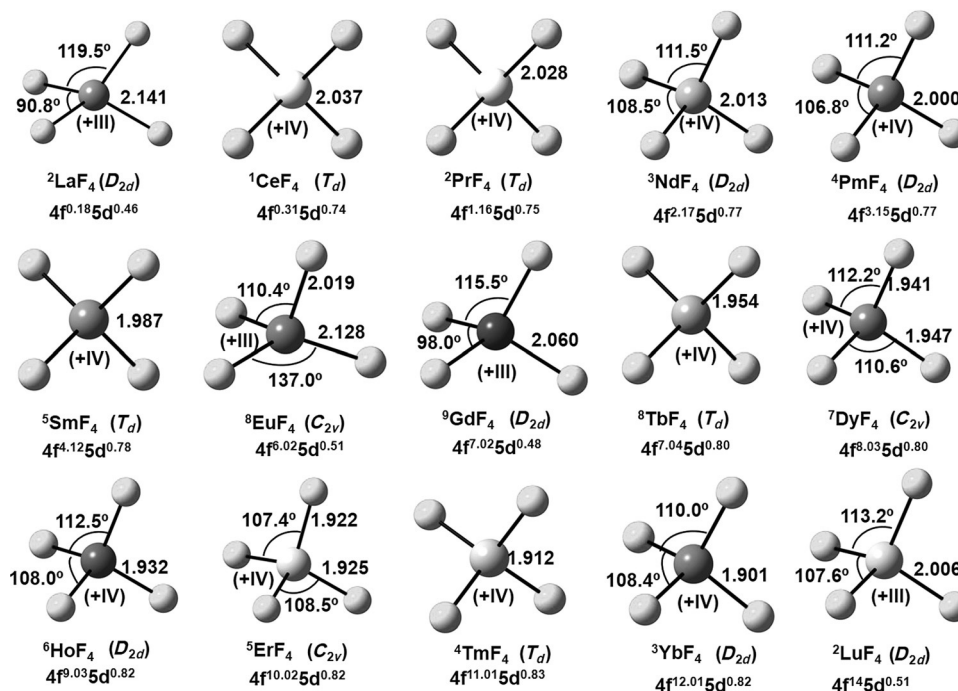

Figure 8. Geometry parameters (Å, degrees), point group, and lanthanide NPA electron configurations at the MP2 level for LnF$_4$.
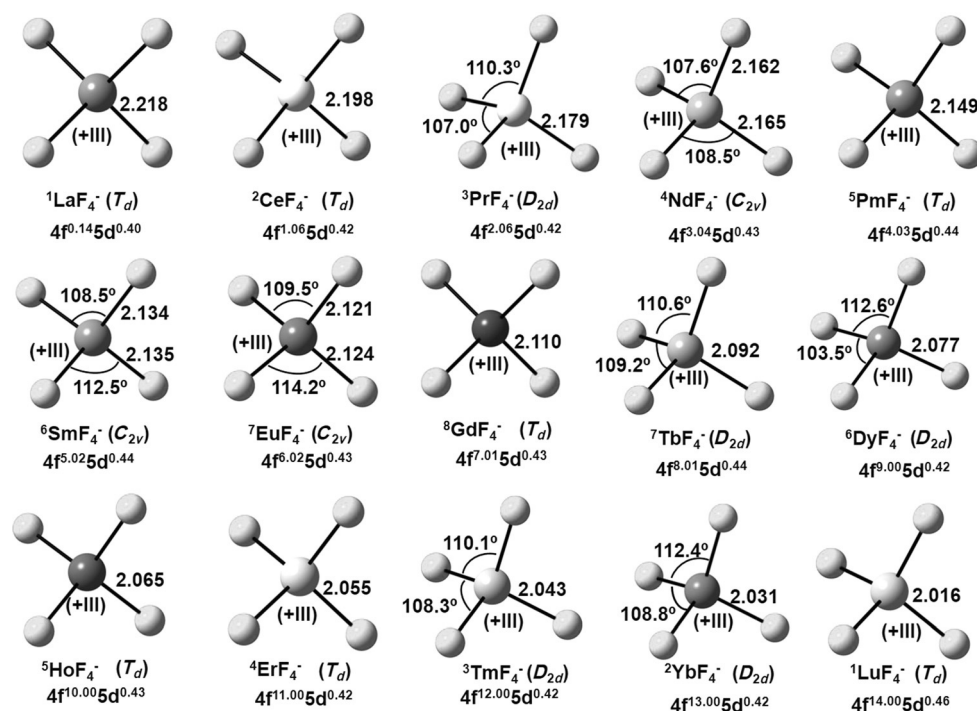
Figure 9. Geometry parameters (Å, degrees), point group, and lanthanide NPA electron configurations at the MP2 level for $[LnF_4]^-$.

distortions from T_d symmetry. In fact, [3]NdF$_4$, [7]DyF$_4$, [6]HoF$_4$, [5]ErF$_4$, and [3]YbF$_4$ are only slightly distorted from a T_d geometry by a few degrees. The distortions from ideal T_d symmetry for the neutral tetrafluorides with Ln in the formal +III oxidation are larger than those for the tetrafluorides with Ln in the formal +IV oxidation state. This difference is, in part, due to one spin being on the fluorine atoms and more ionic Ln−F bonds.

The anionic complexes have longer bonds than their neutral counterparts. The anionic complexes (Figure 9) mostly follow the lanthanide contraction. For these complexes, $[LaF_4]^-$ has the longest bond length with $[LuF_4]^-$ having the shortest. Unlike the neutral complexes, all the geometries for the anionic complexes are tetrahedral or slightly distorted tetrahedral structures.

Vibrational frequencies

The neutral complexes follow the lanthanide contraction for the Ln−F bond lengths, except for high-spin [8]EuF$_4$ and [9]GdF$_4$. Thus, we would expect a trend of increasing stretching frequencies as the atomic number increases across the series. Excluding the exceptions, the symmetric stretching frequencies of the LnF$_4$ (Table 1) derived from the a_1 stretch in T_d symmetry show the trend of increasing frequencies. As long as the distortion from the T_d structure is not too large, the t_2 asymmetric stretching frequencies do not exhibit a large splitting. We averaged the frequencies derived from the t_2 T_d mode, as they are not split by very much, for [3]NdF$_4$, [4]PmF$_4$, [6]EuF$_4$, [7]DyF$_4$, [6]HoF$_4$, [5]ErF$_4$, and [3]YbF$_4$ and obtained the values 597, 606, 615, 642, 649, 666, and 678 cm^{-1}, which fit the expected lanthanide contraction pattern when combined with the other results for the T_d molecules. [2]LaF$_4$, [8]EuF$_4$, [7]GdF$_4$, [9]GdF$_4$, and [2]LuF$_4$ exhibit large

splittings of the asymmetric bands so we cannot average their values. Excluding [7]GdF$_4$, these latter fluorides have the Ln in the +III oxidation state and the distortions from T_d geometries are the largest. We note that prior calculations[50] of the stretching modes for CeF$_4$ at the MP2 level with a different basis set are within a few cm^{-1} of the current values.

Good agreement with the experimental matrix results is found for LnF$_2$ and LnF$_3$, showing the validity of the computational approach (see the Supporting Information). The LnF$_3$ species previously reported at the DFT level are all within 30 cm^{-1} of experiment, except for PrF$_3$ where the calculated values differed from experiment by $\approx$ 50 cm^{-1}. The calculated values do not contain anharmonic corrections and the experimental values should be smaller than those predicted. For the LnF$_4$, good agreement with the assigned asymmetric stretches is found for [1]CeF$_4$ (within 10 cm^{-1}), [2]PrF$_4$ (within 10 cm^{-1} of the Ne results), [8]TbF$_4$ (within 15 cm^{-1}), [7]DyF$_4$ (within 15 cm^{-1}), and for [3]NdF$_4$ (within $\approx$ 30 cm^{-1}). The experimental NdF$_4$ results may not be consistent with the Ln contraction.

We include some of the B3LYP results for the LnF$_4$ in Table 1 for the cases in which spin contamination was not too large. The DFT B3LYP Ln−F bond lengths are predicted to be longer than the MP2 values so the predicted frequencies are smaller. In general, there is significant spin contamination at the density functional theory level with the B3LYP functional and it is difficult to get good agreement with experiment. This seems to arise from too much mixing of the +III and +IV oxidation states as well as too much back-bonding into the 4f orbitals from the ligands.

Consistent with the bond lengths, the vibrational frequencies for $[LnF_4]^-$ show the lanthanide contraction (Figure 9). The symmetric stretching frequencies show a constant and gradual

increase as we move across the lanthanide row. The bond lengths are significantly longer in [LnF$_4$]$^-$ than in LnF$_4$ and, as a consequence, the corresponding Ln$-$F stretching frequencies are significantly lower in the anions. The results in Table 2 show much better agreement between the MP2 and B3LYP values.

Table 2. Calculated symmetric (sym) and asymmetric (asym) Ln$-$F vibrational frequencies (ν, cm^{-1}), infrared intensities (I, km mol^{-1}, in parentheses), and bond lengths (r, Å) of [LnF$_4$]$^-$ complexes at the MP2/Stuttgart/aug-cc-pVDZ and B3LYP/Stuttgart/DZVP2 levels.

[LnF$_4$]$^-$	Point group[a]	Sym. ν MP2	Asym. ν MP2	r (Ln$-$F) B3LYP	Sym. $\nu(I)$ B3LYP	Asym. $\nu(I)$ B3LYP
[^{1}LaF$_4$]$^-$	T_d	465.8 (a$_1$)	422.9 (t$_2$)	2.213	454.0, a$_1$ (0)	411.4, t$_2$ (640)
[^{2}CeF$_4$]$^-$	T_d/C_{2v}	470.1 (a$_1$)	433.0 (t$_2$)	2.193×2	469.9 (0)	429.8 (213)
				2.184×2		429.0 (209)
						421.5 (189)
[^{3}PrF$_4$]$^-$	D_{2d}/C_{2v}	478.2	440.7 (e)	2.171×2	473.4 (0)	436.6 (237)
			442.8	2.171×2		429.4 (200)
						428.0 (193)
[^{4}NdF$_4$]$^-$	C_{2v}/T_d	483.9	447.2	2.160	478.4, a$_1$ (0)	443.1, t$_2$ (614)
			448.4			
			448.7			
[^{5}PmF$_4$]$^-$	T_d	488.2 (a$_1$)	452.2 (t$_2$)	2.145	487.8, a$_1$ (0)	454.1, t$_2$ (617)
[^{6}SmF$_4$]$^-$	C_{2v}	494.2	455.4	2.131×2	488.8 (1)	453.9 (199)
			456.9	2.137×2		452.9 (194)
			466.5			449.5 (186)
[^{7}EuF$_4$]$^-$	C_{2v}	498.3	461.1	2.122×2	491.9 (1)	496.3 (192)
			464.1	2.124×2		455.1 (184)
			468.4			452.2 (165)
[^{8}GdF$_4$]$^-$	T_d	502.0 (a$_1$)	467.0 (t$_2$)	2.126	473.9, a$_1$ (0)	448.0, t$_2$ (440)
[^{7}TbF$_4$]$^-$	D_{2d}/T_d	506.8	480.1	2.092	501.6 (0)	465.9, t$_2$ (524)
			473.4 (e)			
[^{6}DyF$_4$]$^-$	D_{2d}/C_{2v}	511.9	471.5 (e)	2.081×2	500.7 (1)	471.1 (187)
			483.6	2.085×2		467.3 (162)
						464.5 (166)
[^{5}HoF$_4$]$^-$	T_d/C_{2v}	513.7 (a$_1$)	481.1 (t$_2$)	2.079×2	509.6 (2)	478.1 (177)
				2.074×2		477.3 (166)
						473.8 (154)
[^{4}ErF$_4$]$^-$	T_d/C_{2v}	516.2	488.3 (t$_2$)	2.065×2	511.6 (2)	486.4 (178)
				2.067×2		481.9 (148)
						479.9 (152)
[^{3}TmF$_4$]$^-$	D_{2d}/C_{2v}	520.6	493.4 (e)	2.050×2	515.1 (8)	486.9 (147)
			494.0	2.059×2		485.1 (155)
						483.3 (158)
[^{2}YbF$_4$]$^-$	D_{2d}	524.3	496.2 (e)	2.043	518.4 (0)	500.3 (158)
			504.4			488.2, e (289)
[^{1}LuF$_4$]$^-$	T_d	531.8 (a$_1$)	505.8 (t$_2$)	2.031	525.7, a$_1$ (0)	500.8, t$_2$ (452)

[a] MP2/B3LYP if they predict different point groups.

Population analysis

A natural population analysis (NPA) using the natural bond orbitals (NBOs) was performed to analyze the electron configurations of the lanthanides. There is minimal spin contamination for most compounds at the MP2 level. The spin densities are shown in the Supporting Information. The data for the LnF$_4$ in Table 3 show that La^{III}F$_4$ and Lu^{III}F$_4$ have doublet spin states

Table 3. MP2/Stuttgart/aug-cc-pVDZ population analysis for LnF$_4$

LnF$_4$	S^2/$\langle S^2 \rangle$	Ln excess spin	Ln oxidation state	Ln 4f α	Ln 5d α	Pop 2p F	F 2p $\alpha-\beta$
^{2}LaF$_4$	0.81/0.75		+III	0.08	0.18	2p$^{5.65}$	0.25
^{1}CeF$_4$	0.00/0.00		+IV			2p$^{5.77}$	0
^{2}PrF$_4$	0.75/0.75	4f^1	+IV	1.06	0.38	2p$^{5.77}$	0
^{3}NdF$_4$	2.00/2.00	4f^2	+IV	2.06	0.39	2p$^{5.76}$	0
^{4}PmF$_4$	3.75/3.75	4f^3	+IV	3.05	0.40	2p$^{5.78}$	0
^{5}SmF$_4$	6.01/6.00	4f^4	+IV	4.04	0.41	2p$^{5.79}$	0
^{6}EuF$_4$	8.76/8.75	4f^5	+IV	5.04	0.41	2p$^{5.79}$	0
^{8}EuF$_4$	15.82/15.75	4f^6	+III	6.00	0.23	2p$^{5.42/5.85}$	0.52/0
^{7}GdF$_4$	12.01/12.00	4f^6	+IV	6.03	0.43	2p$^{5.80}$	0
^{9}GdF$_4$	20.05/20.00	4f^7	+III	7.00	0.20	2p$^{5.65}$	0.25
^{8}TbF$_4$	15.76/15.75	4f^7	+IV	7.00	0.43	2p$^{5.80}$	0
^{7}DyF$_4$	12.01/12.00	4f^6	+IV	7.00	0.42	2p$^{5.80}$	0
^{6}HoF$_4$	8.76/8.75	4f^5	+IV	7.00	0.43	2p$^{5.80}$	0
^{5}ErF$_4$	6.01/6.00	4f^4	+IV	7.00	0.43	2p$^{5.80}$	0
^{4}TmF$_4$	3.75/3.75	4f^3	+IV	7.00	0.42	2p$^{5.80}$	0
^{3}YbF$_4$	2.00/2.00	4f^2	+IV	7.00	0.42	2p$^{5.80}$	0
^{2}LuF$_4$	0.82/0.75		+III	7.00	0.19	2p$^{5.63}$	0.29

with the one spin on the fluorine atoms as the f orbitals are formally empty or completely filled; these end point limiting cases are in the +III oxidation state. Most of the remaining Ln are in the +IV oxidation state with all of the spin localized on the Ln. Except for high-spin ^{8}EuF$_4$ and ^{9}GdF$_4$, there is ≈0.8 e in the d orbitals, which is predominantly spin paired. This represents back-donation from the F ligands to the Ln. There is a small amount of back-bonding into the 4f orbitals on most of the Ln up to 0.3 e. The largest back-bonding to the 4f orbital is for Ce. There is very little back-bonding to the 4f orbital past Sm. For the high-spin ^{8}EuF$_4$ and ^{9}GdF$_4$, there is substantially less back-bonding to the 5d orbitals from the F atoms with only ≈0.5 e in the 5d orbitals. For the high-spin ^{8}EuF$_4$ and ^{9}GdF$_4$, the oxidation state is +III, with one unpaired spin on the F atoms, which is either fully shared on all four atoms as in ^{9}GdF$_4$, ^{2}LaF$_4$, and ^{2}LuF$_4$, or localized on two F atoms as in ^{8}EuF$_4$. For high-spin ^{8}EuF$_4$, the molecule has a 4f^6 open-shell configuration on the Eu. For ^{9}GdF$_4$, the Gd has a 4f^7 configuration. Thus, for these two high-spin cases where it is possible to attain a half-filled or close to half-filled shell, the tetrafluoride prefers the +III oxidation state. We note that this preference is only by 4 kcal mol^{-1} for EuF$_4$, which does not attain the 4f^7 electronic configuration.

The NBO analysis shows that the Ln$-$F bonds are highly ionic. For LnF$_4$ with Ln in the formal +III oxidation state (Ln = La, Eu, Gd, Lu), the Ln$-$F bond is almost completely ionic and there is an excess spin density on the fluorine atoms. For LnF$_4$

with Ln in the formal +IV oxidation state, there is only 6–8% of the population on the Ln. The Ln contribution has ≈30% from the 4f orbitals and 64% from the 5d orbitals with ≈6% from the 6s orbital for Ce, Pr, and Nd. For PmF$_4$, the participation of Pm 4f electrons drops to 12% and further drops to 3–7% for the remaining Ln^{IV}. The majority valence orbital contribution of ≈70% is from the Ln 5d orbitals and the remainder is from the 6s.

In contrast, the B3LYP calculation results have more 4f orbital character than do the MP2 calculations with the 4f orbitals being involved in the back-bonding from the F ligands. This could be the cause of some of the difficulties with spin contamination in the open-shell calculations. The significant spin contamination can arise as the Ln tries to mix different electron occupancies and oxidation states.

The NPA data for the anions are given in Table 4. In this case, all of the anions are in the +III oxidation state. There is no excess spin on any of the F atoms in contrast to the neutral compounds. Thus, when an electron is added to LnF$_4$, it goes into an f orbital on the Ln if it is available.

Table 4. MP2/Stuttgart/aug-cc-pVDZ population analysis for [LnF$_4$]$^-$.

[LnF$_4$]$^-$	$S^2/\langle S^2\rangle$	Ln excess spin	Ln oxidation state	Ln 4f α	Ln 5d α	Pop 2p F
[^{1}LaF$_4$]$^-$	0.00/0.00		+III			2p$^{5.89}$
[^{2}CeF$_4$]$^-$	0.75/0.75	4f^1	+III	1.02	0.21	2p$^{5.88}$
[^{3}PrF$_4$]$^-$	2.00/2.00	4f^2	+III	2.02	0.22	2p$^{5.89}$
[^{4}NdF$_4$]$^-$	3.75/3.75	4f^3	+III	3.01	0.22	2p$^{5.90}$
[^{5}PmF$_4$]$^-$	6.00/6.00	4f^4	+III	4.01	0.23	2p$^{5.90}$
[^{6}SmF$_4$]$^-$	8.76/8.75	4f^5	+III	5.00	0.23	2p$^{5.90}$
[^{7}EuF$_4$]$^-$	12.00/12.00	4f^6	+III	6.00	0.23	2p$^{5.90}$
[^{8}GdF$_4$]$^-$	15.76/15.75	4f^7	+III	7.00	0.23	2p$^{5.90}$
[^{7}TbF$_4$]$^-$	12.01/12.00	4f^6	+III	7.00	0.23	2p$^{5.90}$
[^{6}DyF$_4$]$^-$	8.76/8.75	4f^5	+III	7.00	0.22	2p$^{5.90}$
[^{5}HoF$_4$]$^-$	6.00/6.00	4f^4	+III	7.00	0.22	2p$^{5.90}$
[^{4}ErF$_4$]$^-$	3.75/3.75	4f^3	+III	7.00	0.22	2p$^{5.90}$
[^{3}TmF$_4$]$^-$	2.00/2.00	4f^2	+III	7.00	0.21	2p$^{5.90}$
[^{2}YbF$_4$]$^-$	0.75/0.75	4f^1	+III	7.00	0.21	2p$^{5.90}$
[^{1}LuF$_4$]$^-$	0.00/0.00		+III			2p$^{5.89}$

Reaction energies

Various energy quantities are summarized in Table 5. The electron affinities of the LnF$_4$ are, in general, very high, showing that these compounds will be excellent oxidizing agents. These electron affinities range from 2.67–9.65 eV, and some of these electron affinities are extraordinarily high, substantially larger than the electron affinity range of the halogen atoms (3.0–3.6 eV). These high electron affinities suggest that the most of the neutral LnF$_4$ complexes can act as enhanced oxidizing agents. CeF$_4$ has the lowest electron affinity owing to it being a closed-shell singlet. The electron affinities increase from CeF$_4$ to EuF$_4$. Most of the remaining electron affinities are in the 6.0 to 10.0 eV range, except for TbF$_4$ and DyF$_4$ with lower electron affinities near 4 eV. TbF$_4$ has a stabilized, completely half-full subshell so the neutral species is more stable,

Table 5. Calculated electron affinities, fluoride affinities, F$_2$ elimination energies, and Ln—F BDE at the MP2/Stuttgart/aug-cc-pVDZ level.

LnF$_4$	Electron affinity [eV] (0 K)	Fluoride affinity LnF$_3$+F$^-$ → [LnF$_4$]$^-$ [kcal mol^{-1}] (298 K)	F$_2$ elimination LnF$_4$ → LnF$_2$+F$_2$ [kcal mol^{-1}] (298 K)	Ln—F BDE LnF$_4$ → LnF$_3$+F [kcal mol^{-1}] (298 K)
^{2}LaF$_4$	7.78	97.1	124.4	−0.5
^{1}CeF$_4$	2.67	93.3	268.3	113.8
^{2}PrF$_4$	4.91	94.2	205.1	62.9
^{3}NdF$_4$	6.38	94.7	153.2	29.6
^{4}PmF$_4$	7.05	103.3	145.9	22.7
^{5}SmF$_4$	7.43	100.6	133.3	11.3
^{8}EuF$_4$[a]	8.48	100.8	56.1	−12.9
^{9}GdF$_4$	8.20	106.0	113.3	−1.5
^{8}TbF$_4$	3.99	104.3	279.4[b]	94.5
^{7}DyF$_4$	3.94	84.7	174.1[b]	76.0
^{6}HoF$_4$	6.04	87.5	134.7	30.3
^{5}ErF$_4$	8.10	111.7	120.3	7.0
^{4}TmF$_4$	8.21	108.3	82.6	1.0
^{3}YbF$_4$	9.65	107.6	22.4	−32.7
^{2}LuF$_4$	8.52	112.6	119.1	−2.3

[a] For ^{6}EuF$_4$, EA = 8.71 eV, E(F$_2$ elimination) = 51.1 kcal mol^{-1}, Ln—F BDE = −17.9 kcal mol^{-1}. [b] There is significant spin contamination for TbF$_2$ and DyF$_2$.

lowering the electron affinity. DyF$_4$ may be starting a new sequence like PrF$_4$.

The Ln—F bond dissociation energies (BDEs) are probably lower than expected owing to the use of MP2 to calculate these values. The only available data is for the average BDE of CeF$_4$, which is 144 kcal mol^{-1}.[50] The highest Ln—F BDE belongs to CeF$_4$, because CeF$_4$ is a closed-shell singlet in its ground state. ^{2}LaF$_4$, ^{8}EuF$_4$, ^{9}GdF$_4$, ^{3}YbF$_4$, and ^{2}LuF$_4$ are predicted to have negative BDEs. Even if there is an error at the MP2 level, these BDEs will still be low. For LaF$_4$, the Ln cannot attain the +IV oxidation state so the BDE should be small or near zero, as found. Again, ^{8}EuF$_4$ and ^{9}GdF$_4$ have the Ln in the +III oxidation state and they do not want to bind the additional F to LnF$_3$. CeF$_4$, PrF$_4$, NdF$_4$, TbF$_4$, and DyF$_4$ have all been observed. In this group of tetrafluorides, except for NdF$_4$, all of the predicted Ln—F BDEs are substantial consistent with the observation of these compounds. The NdF$_4$ BDE near 30 kcal mol^{-1} must be just enough for the compound to be stable as it has been observed. In contrast, SmF$_4$ with a ≈20 kcal mol^{-1} lower BDE was not observed. The calculated results suggest that HoF$_4$ might be possible to observe.

The F$_2$ elimination reaction energies show that many of these compounds should be very stable with respect to loss of F$_2$ to form LnF$_2$ with the Ln in the +II oxidation state. The highest F$_2$ elimination belongs to CeF$_4$ because Ce^{IV} is a closed-shell singlet and requires more energy to remove fluorine and produce the less stable +II oxidation state. The lowest F$_2$ elimination reaction energy belongs to YbF$_4$, which is consistent with the negative Yb—F BDE. EuF$_4$ is also predicted to be not very stable with respect to loss of F$_2$, again consistent with the Eu—F BDE.

CHEMISTRY
A European Journal
Full Paper

Conclusion

We report the matrix-isolated reaction products of laser-ablated lanthanide atoms with fluorine in excess neon and argon. Our argon and neon experimental results are supported by experiments in neat fluorine matrices. Besides the known tetrafluorides of Ce, Pr, and Tb, the new neutral NdF_4 and DyF_4 molecules were observed and characterized by IR spectroscopy. There is no evidence of tetrafluoride formation for Sm and Ho. This is consistent with the low Sm—F BDEs. The Ho—F BDE is predicted to be comparable to the Nd—F BDE, but we did not observe HoF_4 whereas NdF_4 was observed. PrF_4 and TbF_4 have lower BDEs than for CeF_4, consistent with the decomposition of the former two in the vapor.[21] The tetrafluorides in the middle of the period (Sm, Eu, and Gd), those near the end of the period (Er, Tm, Yb, and Lu), and La at the beginning of the period are likely not to be synthesized owing to the low Ln—F BDEs. This shows that the $+$III oxidation is clearly preferred for these Ln over the $+$IV. The population analysis shows that, except for La, Eu, Gd, and Lu, the tetrafluorides all prefer the $+$IV oxidation state. The ones noted still prefer the $+$III oxidation state for the tetrafluoride. The calculations further show that the observed LnF_4 species are very stable against loss of F_2. The Ln in the $+$IV oxidation state have approximately 0.8 e in the 5d orbitals as a result of back-bonding from the F ligands, whereas those in the $+$III oxidation state have approximately 0.5 e in the 5d orbitals. The early Ln up to Sm have some back-bonding into the 4f orbitals, but after Sm, there is essentially no back-bonding into the 4f orbitals. The tetrafluorides in the $+$IV oxidation state, excluding CeF_4, differ from the $OLnF_2$ compounds, which are in the $+$III oxidation state or in a mixed $+$III/$+$IV oxidation state (Pr and Tb). Addition of an electron to LnF_4 or, equivalently, addition of F^- to LnF_3, leads to the Ln being in the $+$III oxidation state for all of the $[LnF_4]^-$. The $[LnF_4]^-$ anions have about 0.45 e in the 5d orbitals as a result of back-bonding and there is essentially no back-bonding to the 4f orbitals. The calculated electron affinities verify that the LnF_4 species are strong oxidizing agents and, in fact, would have some of the highest known electron affinities if they could be synthesized. Not surprisingly, the stable, observed LnF_4 have the lower electron affinities. The calculated fluoride affinities show that the LnF_3 are moderate to strong Lewis acids and that it should be possible to generate most of the $[LnF_4]^-$ anions as they are very stable to loss of an electron. In addition to the tetrafluorides, the trifluorides were also observed and further characterized and some difluorides were observed.

Acknowledgments

[1] T. Tsuchiya, T. Taketsugu, H. Nakano, K. Hirao, *J. Mol. Struct.* **1999**, *461–462*, 203–222.
[2] R. D. Wesley, C. W. DeKock, *J. Chem. Phys.* **1971**, *55*, 3866–3877.
[3] M. Lesiecki, J. W. Nibler, C. W. DeKock, *J. Chem. Phys.* **1972**, *57*, 1352–1353.
[4] M. Hargittai, *Coord. Chem. Rev.* **1988**, *91*, 35–88.
[5] L. Joubert, G. Picard, J.-J. Legendre, *Inorg. Chem.* **1998**, *37*, 1984–1991.
[6] G. Lanza, C. Minichino, *ChemPhysChem* **2009**, *10*, 507–511.
[7] S. Tsukamoto, H. Mori, H. Tatewaki, E. Miyoshi, *Chem. Phys. Lett.* **2009**, *474*, 28–32.
[8] A. Weigand, X. Cao, J. Yang, M. Dolg, *Theor. Chem. Acc.* **2010**, *126*, 117–127.
[9] E. W. Kaiser, W. E. Falconer, W. Klemperer, *J. Chem. Phys.* **1972**, *56*, 5392–5398.
[10] R. H. Hauge, J. W. Hastie, J. L. Margrave, *J. Less-Common Met.* **1971**, *23*, 359–365.
[11] J. W. Hastie, R. H. Hauge, J. L. Margrave, *J. Less-Common Met.* **1975**, *39*, 309–334.
[12] M. Chen, D. A. Dixon, X. Wang, H.-G. Cho, L. Andrews, *J. Phys. Chem. A* **2011**, *115*, 5609–5624.
[13] M. R. MacDonald, J. W. Ziller, W. J. Evans, M. R. MacDonald, J. W. Ziller, W. J. Evans, *J. Am. Chem. Soc.* **2011**, *133*, 15914–15917.
[14] M. R. MacDonald, J. E. Bates, M. E. Fieser, J. W. Ziller, F. Furche, W. J. Evans, *J. Am. Chem. Soc.* **2012**, *134*, 8420–8423.
[15] M. R. MacDonald, J. E. Bates, M. E. Fieser, J. W. Ziller, F. Furche, W. J. Evans, *J. Am. Chem. Soc.* **2013**, *135*, 9857–9868.
[16] G. Meyer, *Angew. Chem. Int. Ed.* **2014**, *53*, 3550–3551; *Angew. Chem.* **2014**, *126*, 3620–3622.
[17] J. W. Hastie, R. H. Hauge, J. L. Margrave, *High Temp. Sci.* **1971**, *3*, 56–72.
[18] N. N. Greenwood, A. Earnshaw, *Chemistry of the Elements*, Chapter 30, Pergamon Press, Oxford, **1994**, pp. 1423–1449.
[19] Z. Mazej, *J. Fluorine Chem.* **2002**, *118*, 127–129.
[20] V. I. Spitsyn, Y. M. Kiselev, L. I. Martynenko, V. N. Prusakov, V. B. Sokolov, *Dokl. Akad. Nauk SSSR* **1974**, *219*, 621–624.
[21] E. W. Kaiser, W. A. Sunder, W. E. Falconer, *J. Less-Common Met.* **1972**, *27*, 383–387.
[22] L. R. Batsanova, Y. V. Zakhar'ev, A. A. Alovskii, *Zh. Neorg. Khim.* **1973**, *18*, 905–908.
[23] S. D. Gabelnick, G. T. Reedy, M. G. Chasanov, *J. Chem. Phys.* **1974**, *60*, 1167–1171.
[24] T. Mikulas, M. Chen, D. A. Dixon, K. A. Peterson, Y. Gong, L. Andrews, *Inorg. Chem.* **2014**, *53*, 446–456.
[25] R. Hoppe, *Rare Earths Mod. Sci. Technol.* **1982**, *3*, 315–316.
[26] Z. Hu, G. Kaindl, B. G. Mueller, *J. Alloys Compd.* **1997**, *246*, 177–185.
[27] T. Vent-Schmidt, S. Riedel, *Inorg. Chem.* **2015**, *54*, 11114–11120.
[28] X. Wang, H.-G. Cho, L. Andrews, M. Chen, D. A. Dixon, H.-S. Hu, J. Li, *J. Phys. Chem. A* **2011**, *115*, 1913–1921.
[29] Y. Gong, X. Wang, L. Andrews, M. Chen, D. A. Dixon, *Organometallics* **2011**, *30*, 4443–4452.
[30] Y. Gong, L. Andrews, M. Chen, D. A. Dixon, *J. Phys. Chem. A* **2011**, *115*, 14581–14592.
[31] R. G. Parr, W. Yang, *Density-Functional Theory of Atoms and Molecules*, Oxford University Press, New York, **1989**.
[32] A. D. Becke, *J. Chem. Phys.* **1993**, *98*, 5648–5652.
[33] C. Lee, W. Yang, R. G. Parr, *Phys. Rev. B* **1988**, *37*, 785–789.
[34] N. Godbout, D. R. Salahub, J. Andzelm, E. Wimmer, *Can. J. Chem.* **1992**, *70*, 560–571.
[35] M. Dolg, H. Stoll, H. Preuss, *J. Chem. Phys.* **1989**, *90*, 1730.
[36] X. Cao, M. Dolg, *J. Mol. Struct.* **2002**, *581*, 139–147.
[37] C. Møller, M. S. Plesset, *Phys. Rev.* **1934**, *46*, 618–622.

[38] J. A. Pople, J. S. Binkley, R. Seeger, *Int. J. Quantum Chem. Symp.* **2009**, *10*, 1–19.

[39] R. A. Kendall, T. H. Dunning Jr., R. J. Harrison, *J. Chem. Phys.* **1992**, *96*, 6796–6806.

[40] E. D. Glendening, C. R. Landis, F. Weinhold, *J. Comput. Chem.* **2013**, *34*, 1429–1437; NBO 6.0: Natural Bond Orbital Analysis Program.

[41] E. D. Glendening, J. K. Badenhoop, A. E. Reed, J. E. Carpenter, J. A. Bohmann, C. M. Morales, C. R. Landis, F. Weinhold, http://nbo6.chem.wisc.edu/, Theoretical Chemistry Institute, University of Wisconsin, Madison, WI, **2013**.

[42] F. Weinhold, in *Encyclopedia of Computational Chemistry, Vol. 3* (Ed.: P. v. R. Schleyer), John Wiley & Sons, Chichester, **1998**, pp. 1792–1811.

[43] F. Weinhold, C. R. Landis, *Valency and Bonding: A Natural Bond Orbital Donor–Acceptor Perspective*, University Press, Cambridge, **2005**.

[44] A. E. Reed, L. A. Curtiss, F. Weinhold, *Chem. Rev.* **1988**, *88*, 899–926.

[45] Gaussian 09, Revision D.01, M. J. Frisch, G. W. Trucks, H. B. Schlegel, G. E. Scuseria, M. A. Robb, J. R. Cheeseman, G. Scalmani, V. Barone, B. Mennucci, G. A. Petersson, H. Nakatsuji, M. Caricato, X. Li, H. P. Hratchian, A. F. Izmaylov, J. Bloino, G. Zheng, J. L. Sonnenberg, M. Hada, M. Ehara, K. Toyota, R. Fukuda, J. Hasegawa, M. Ishida, T. Nakajima, Y. Honda, O. Kitao, H. Nakai, T. Vreven, J. A. Montgomery, Jr., J. E. Peralta, F. Ogliaro, M. Bearpark, J. J. Heyd, E. Brothers, K. N. Kudin, V. N. Staroverov, R. Kobayashi, J. Normand, K. Raghavachari, A. Rendell, J. C. Burant, S. S. Iyengar, J. Tomasi, M. Cossi, N. Rega, N. J. Millam, M. Klene, J. E. Knox, J. B. Cross, V. Bakken, C. Adamo, J. Jaramillo, R. Gomperts, R. E. Stratmann, O. Yazyev, A. J. Austin, R. Cammi, C. Pomelli, J. W. Ochterski, R. L. Martin, K. Morokuma, V. G. Zakrzewski, G. A. Voth, P. Salvador, J. J. Dannenberg, S. Dapprich, A. D. Daniels, Ö. Farkas, J. B. Foresman, J. V. Ortiz, J. Cioslowski, D. J. Fox, Gaussian, Inc., Wallingford, CT, **2009**.

[46] S. Riedel, T. Koechner, X. Wang, L. Andrews, *Inorg. Chem.* **2010**, *49*, 7156–7164.

[47] T. Vent-Schmidt, F. Brosi, J. Metzger, T. Schloeder, X. Wang, L. Andrews, C. Mueller, H. Beckers, S. Riedel, *Angew. Chem. Int. Ed.* **2015**, *54*, 8279–8283; *Angew. Chem.* **2015**, *127*, 8397–8401.

[48] F. Brosi, T. Vent-Schmidt, S. Kieninger, T. Schlöder, H. T. Beckers, S. Riedel, *Chem. Eur. J.* **2015**, *21*, 16455–16462.

[49] V. N. Bukhmarina, A. Y. Gerasimov, Y. B. Predtechenskii, V. G. Shklyarik, *Opt. Spektrosk.* **1992**, *72*, 69–74.

[50] K. S. Thanthiriwatte, M. Vasiliu, S. R. Battey, Q. Lu, K. A. Peterson, L. Andrews, D. A. Dixon, *J. Phys. Chem. A* **2015**, *119*, 5790–5803.

[51] J. Saloni, S. Roszak, K. Hilpert, M. Miller, J. Leszczynski, *Eur. J. Inorg. Chem.* **2004**, 1212–1218.

[52] L. Bencze, A. Feltrin, S. Nunziante-Cesaro, A. Popovic, *Rapid Commun. Mass Spectrom.* **1996**, *10*, 1248–1258.